ACCOUNTS of chemical research

pubs.acs.org/accounts Article

Increasing Complexity Approach to the Fundamental Surface and Interface Chemistry on SOFC Anode Materials

Simon Penner,* Thomas Götsch, and Bernhard Klötzer

Cite This: *Acc. Chem. Res.* 2020, 53, 1811−1821 Read Online

ACCESS | Metrics & More | Article Recommendations

CONSPECTUS: In this Account, we demonstrate an increasing complexity approach to gain insight into the principal aspects of the surface and interface chemistry and catalysis of solid oxide fuel cell (SOFC) anode and electrolyte materials based on selected oxide, intermetallic, and metal−oxide systems at different levels of material complexity, as well as into the fundamental microkinetic reaction steps and intermediates at catalytically active surface and interface sites. To dismantle the complexity, we highlight our deconstructing step-by-step approach, which allows one to deduce synergistic properties of complex composite materials from the individual surface catalytic properties of the single constituents, representing the lowest complexity level: pure oxides and pure metallic materials. Upon mixing and doping the latter, directly leading to formation of intermetallic compounds/alloys in the case of metals and oxygen ion conductors/mixed ionic and electronic conductors for oxides, a second complexity level is reached. Finally, the introduction of an (inter)metall(ic)−(mixed) oxide interface leads to the third complexity level. A shell-like model featuring three levels of complexity with the unveiled surface and interface chemistry at its core evolves. As the shift to increased complexity decreases the number of different materials, the interconnections between the studied materials become more convoluted, but the resulting picture of surface chemistry becomes clearer. The materials featured in our investigations are all either already used technologically important or prospective components of SOFCs (such as yttria-stabilized zirconia, perovskites, or Ni−Cu alloys) or their basic constituents (e.g., ZrO_2), or they are formed by reactions of other compounds (for instance, pyrochlores are thought to be formed at the YSZ/perovskite phase boundary). We elaborate three representative case studies based on ZrO_2, Y_2O_3, and Y-doped ZrO_2 in detail from all three complexity levels. By interconnection of results, we are able to derive common principles of the influence of surface and interface chemistry on the catalytic operation of SOFC anode materials. *In situ* measurements of the reactivity of water and carbon surface species on ZrO_2- and Y_2O_3-based materials represent levels 1 and 2. The highest degree of complexity at level 3 is exemplified by combined surface science and catalytic studies of metal−oxide systems, oxidatively derived from intermetallic Cu−Zr and Pd−Zr compounds and featuring a large number of phases and interfaces. We show that only by appreciating insight into the basic building blocks of the catalyst materials at lower levels, a full understanding of the catalytic operation of the most complex materials at the highest level is possible.

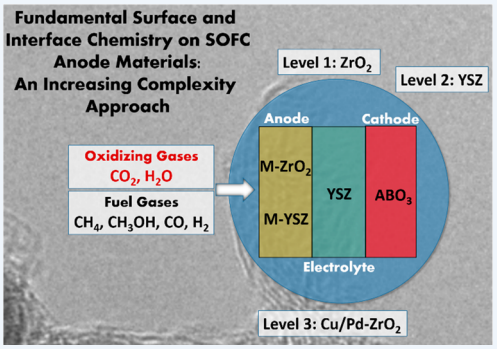

KEY REFERENCES

- Köck, E.-M.; Kogler, M.; Klötzer, B.; Noisternig, M. F.; Penner, S. Structural and Electrochemical Properties of Physisorbed and Chemisorbed Water Layers on the Ceramic Oxides Y_2O_3, YSZ, and ZrO_2. *ACS Appl. Mater. Interfaces* **2016**, *8*, 16428−16443.[1] *Combined in situ infrared and electrochemical impedance spectroscopy revealed the complex interplay of water with the surfaces of SOFC-relevant oxides.*
- Kogler, M.; Köck, E.-M.; Perfler, L.; Bielz, T.; Stöger-Pollach, M.; Hetaba, W.; Willinger, M.; Huang, X.; Schuster, M.; Klötzer, B.; Penner, S. Methane Decomposition and Carbon Growth on Y_2O_3, Yttria-Stabilized Zirconia, and ZrO_2. *Chem. Mater.* **2014**, *26*, 1690−1701.[2] *By a combination of in situ spectroscopy and structural characterization, we revealed the propensity of pure oxide surfaces to coking effects following hydrocarbon treatment at high temperatures.*
- Kogler, M.; Köck, E.-M.; Klötzer, B.; Perfler, L.; Penner, S. Surface Reactivity of YSZ, Y_2O_3 and ZrO_2 toward CO, CO_2 and CH_4: A Comparative Discussion. *J. Phys. Chem. C* **2016**, *120*, 3882−3898.[3] *Using C1 model gas molecules, the interlink between surface chemistry and electrochemical*

Received: April 18, 2020
Published: August 12, 2020

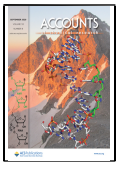

https://dx.doi.org/10.1021/acs.accounts.0c00218
Acc. Chem. Res. 2020, 53, 1811−1821

properties via adsorbate- and carburization-induced conductivity processes was revealed by combined in situ infrared and electrochemical impedance spectroscopy.

- Mayr, L.; Köpfle, N.; Klötzer, B.; Götsch, T.; Bernardi, J.; Schwarz, S.; Keilhauer, T.; Armbrüster, M.; Penner, S. Microstructural and Chemical Evolution and Analysis of a Self-Activating CO_2-Selective Cu−Zr Bimetallic Methanol Steam Reforming Catalyst. *J. Phys. Chem. C* **2016**, *120*, 25395−25404.[4] *Decomposition of a $Cu_{51}Zr_{14}$intermetallic compound in a methanol steam reforming mixture by self-activation was revealed to cause formation of a highly CO_2-selective Cu/t-ZrO_2catalyst.*

INTRODUCTION

Although solid oxide fuel cells (SOFCs) are part of the prospective energy infrastructure, some challenges in their adaption still remain. Besides the need for lower operating temperatures, fuels that are easier to store, cheaper, and/or more abundant than hydrogen are preferred. While external reformers enable the transformation of various compounds into hydrogen and carbon monoxide,[5] the environmental footprints of such systems are drastic. Alternatively, the anode can act as an internal reforming catalyst,[6,7] allowing to feed the fuel (mixed with either H_2O or CO_2) directly to the anode. At the same time, the dimensions of the whole SOFC unit can be kept as small as possible for nonstationary applications. However, the standard nickel/yttria-stabilized zirconia (YSZ) anode working well in hydrogen and sufficiently water-enriched reformate gas is not ideally suited for the operation in methane-containing feeds as it is susceptible to deactivation by coking.[8−11] Thus, optimization of internal reforming processes is of prime importance.

In this Account, we demonstrate a typical workflow allowing insight into the fundamental surface chemistry of internal reforming processes by exploiting an increasing material complexity approach using materials on different model-system- and technology-oriented levels. Figure 1 features a sketch of this workflow encompassing the studied materials and their property relations. Concentric circular shells represent the three material complexity levels. Level 1 deals with the simplest systems, i.e., pure oxides and metals such as ZrO_2 or nickel. Level 2 includes mixed materials in the form of alloys and doped or, generally, compositionally/structurally more complex oxides, such as YSZ or perovskites. Some of these oxide materials are ionic conductors for oxygen anions and are rendered with a black border in the sketch. Finally, a metal/oxide interface is introduced by combining metals and (complex) oxides to model supported (cermet) systems (level 3), featuring the highest complexity level due to the large number of different phases and surface sites present under reaction conditions.

Following this sketch, the center can be reached via multiple pathways, starting with the combined knowledge of the single components' surface chemistry. In this Account, we highlight one possible path from our research exemplifying how information can be intertransferred between the material complexity levels. We also highlight how a multitude of complementary *in situ* or *operando* techniques can be efficiently used together to derive common principles of operation.

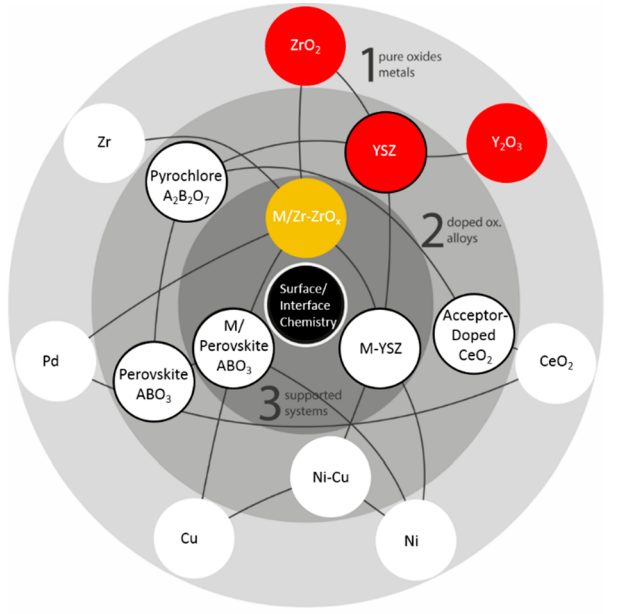

Figure 1. Sketch of the increasing complexity approach. The concentric circles describe the different material complexity levels, with level 1 focusing on the lowest and level 3 representing the highest complexity. Materials with a black border are ionic conductors, and the lines between the different nodes express various connections between the materials in our studies. The colored materials are featured in the three studies presented in this work.

AN EXEMPLARY PATH TO UNRAVEL THE SURFACE AND INTERFACE CHEMISTRY OF REFORMING PROCESSES ON SOFC ANODE MATERIALS

In the next three sections, we describe a typical procedure in our workflow covering all complexity materials levels from the lowest to the highest, starting from simple systems and subsequently adding more complexity to gain information about reforming processes of carbon-based fuels on SOFC anode materials. As a representative example serving as the recurrent theme, we focus on the understanding of water and carbon reactivity on ZrO_2-related materials in reforming reactions. Specifically, we focused on the fundamental understanding of methane steam/dry as well as methanol steam reforming, covering materials from all complexity levels. In this respect, we show that it is highly essential to cover the entire SOFC-relevant temperature axis. Only by connecting information from all complexity levels at realistic temperatures and under realistic gas phase conditions, a clear picture evolves, allowing generalization and intertransformation of knowledge between different materials and reactions. Moving along the material and property complexity axis, we start from the isolated water and carbon reactivity on comparatively simple oxide surfaces (ZrO_2 and Y_2O_3, level 1) and continue via changes in the water and carbon reactivity on more complex oxides as a function of the doping level (Y-doped ZrO_2, level 2) to the *in situ* corrosion of complex intermetallic compound/alloy materials in methane dry and methanol steam reforming mixtures (Pd_2Zr/Pd_3Zr, Pd−Zr alloy, and $Cu_{51}Zr_{14}$, level 3),

https://dx.doi.org/10.1021/acs.accounts.0c00218
Acc. Chem. Res. 2020, 53, 1811−1821

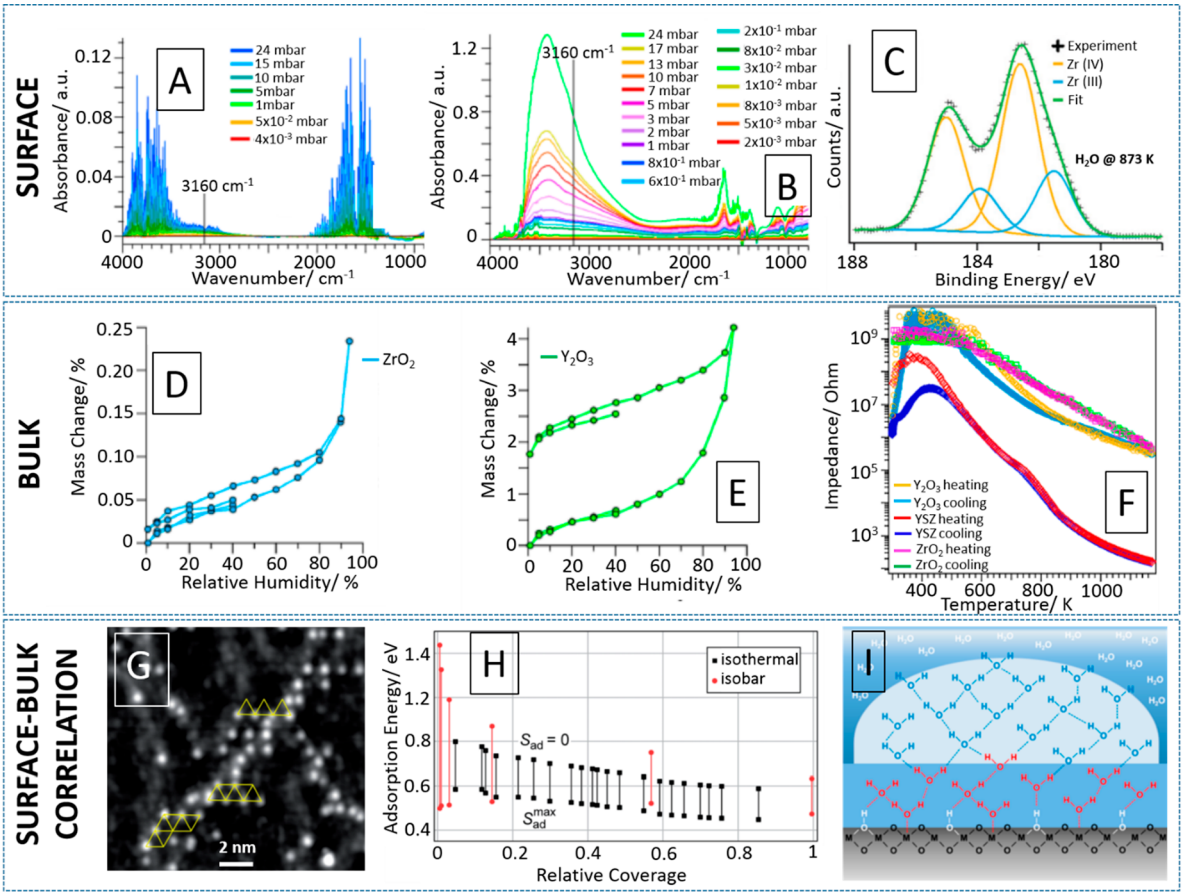

Figure 2. Water reactivity on $ZrO_2$and Y_2O_3: (A, B) *In situ* isothermal FT-IR spectra at variable H_2O pressure on m-ZrO_2 and Y_2O_3. (C) Zr 3d XP spectrum on t-ZrO_2 after water exposure at 873 K. (D, E) Dynamic water sorption measurements on ZrO_2 and Y_2O_3. (F) *In situ* temperature-resolved electrochemical impedance spectra on ZrO_2 and Y_2O_3 under water atmosphere. (G) STM image of an ultrathin ZrO_x film on Pt_3Zr after 15 L water exposure at 293 K. (H) Calculation of the water adsorption energy on m-ZrO_2 from *in situ* isothermal and isobaric FT-IR experiments. (I) Multilayer model for the water adsorption on YSZ. Reproduced with permission from ref 1 (A, B, D–F, I), ref 19 (C), and ref 16 (G, H). Copyright 2020 American Chemical Society, 2017 the Royal Chemical Society, and 2018 the Royal Chemical Society, respectively.

leading to active and selective composite Pd/ZrO_2 and Cu/ZrO_2 systems, respectively. Particular emphasis is given to exemplify how the operation of the most complex Cu/Pd–ZrO_2 interface in reforming reactions can only be understood on the basis of the interaction with water as well as with carbon-containing fuels with the individual building blocks.

LEVEL 1: WATER AND CARBON REACTIVITY ON ZrO_2 AND Y_2O_3: ELUCIDATING THE COMPLEX INTERPLAY BETWEEN (STEAM) REFORMING REACTANTS AND OXIDE SURFACES

As an example, the interaction of water and methane with the surfaces of the insulating oxides (with respect to both electrons and ions) ZrO_2 and Y_2O_3 was investigated separately using *in situ* Fourier-transform infrared (FT-IR) spectroscopy and electrochemical impedance spectroscopy (EIS).[1−3] Brunauer–Emmett–Teller (BET) surfaces of the powder samples differ (2 $m^2\ g^{-1}$ (m-ZrO_2), 32 $m^2\ g^{-1}$ (YSZ), (Y_2O_3)120 $m^2\ g^{-1}$), but according to Barrett–Joyner–Halenda analysis porosity is essentially absent. For both EIS and FT-IR analysis, pressed powder samples are used. ZrO_2 is usually monoclinic (m-), and the tetragonal (t-) polymorph must be stabilized by doping (*e.g.*, YSZ)[12,13] or crystallite size effects.[14] As the metal (*e.g.*, Cu)–t-ZrO_2 interface has been shown to exhibit beneficial reforming properties,[4] a sophisticated synthesis routine to phase-pure t-ZrO_2, pertaining its structure in oxidative, reductive, or reactive gas environments, as long as the temperature is kept below 723 K, was developed to compare the intrinsic surface-chemical behavior of different ZrO_2 polymorphs.[15]

Water Reactivity

The different adsorption behavior of ZrO_2 and Y_2O_3 is already visible in FT-IR spectra acquired as a function of H_2O partial pressure at 298 K (Figure 2A and B). Whereas for pure m-ZrO_2 strongly bonded dissociated water species at the otherwise hydrolysis-inert surface are clearly absent (only terminal and multicoordinated water signals at 3780/3670 cm^{-1} and a sharp δ(OH) peak at 1645 cm^{-1}, strongly masked by gas phase H_2O, are visible at lower water partial pressures[1]), a simple molecular water adsorption model cannot explain the complex water–Y_2O_3 interaction, as dissociative water incorporation into the crystal lattice prevails. Also the superimposed molecular water surface adsorption behavior appears much more complex and involves an array of multicoordinated hydroxyl groups. Surface Zr hydroxylation is also prevalent for t-ZrO_2 treated in water at 873 K (Figure 2C). Minor surface reduction of Zr takes place, but the majority of Zr species appear in a Zr(IV)–OH state (with the Zr $3d_{3/2}$ component measured at 182.5 eV).[1] This example is of particular importance, as it subsequently allows one to address the reversibly formed reactive OH groups of the

https://dx.doi.org/10.1021/acs.accounts.0c00218
Acc. Chem. Res. 2020, 53, 1811−1821

Cu−t-ZrO_2 interface formed by *in situ* decomposition of $Cu_{51}Zr_{14}$ (*cf.* Figure 5A). Dynamic sorption measurements on ZrO_2 and Y_2O_3 (presented via the mass change as a function of the water partial pressure in Figure 2D and E) also show vast adsorption and reactivity differences. m-ZrO_2 adsorbs ultrathin water layers only at the surface, but Y_2O_3 adsorbs more than 4% of its mass, revealing a strong adsorption hysteresis effect. *In situ* EIS data acquired during water adsorption on both samples show only a limited increase in conductivity (Figure 2F). This indicates that, despite their vastly different nature, both the strongly and irreversibly dehydroxylated pure m-ZrO_2 (exhibiting unreactive isolated OH groups) and the ice- and polymeric chainlike water layers on Y_2O_3 hardly show any proton conductivity up to 1173 K. To connect surface and bulk properties, Figure 2G shows a scanning tunneling microscopy (STM) image of an ultrathin ZrO_x film on a Pt_3Zr single crystal,[16] exposed to 15 Langmuir equivalents of H_2O at 293 K. Water-related species are found preferentially above subsurface dislocation lines (gray areas in the image) showing strong local ordering (yellow triangles). Correlated FT-IR data on m-ZrO_2 yield a strikingly similar range for molecular water adsorption energies around 0.57 eV as compared to the complementary surface-science and density functional theory studies, highlighting the strong potential of our dedicated "materials gap-bridging" approach in resolving reactivity issues on structurally strongly different bulk- and surface phases of ZrO_2.[16] Figures 2I and 3 summarize the derived general picture and differences of

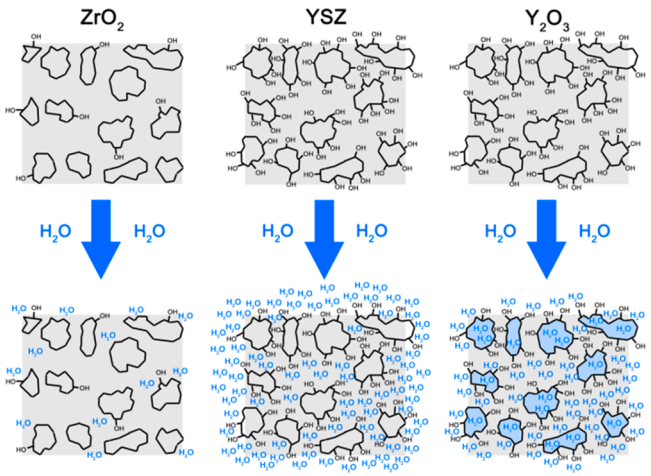

Figure 3. Schematic comparison of different water adsorption on m-ZrO_2, Y_2O_3, and YSZ. Reproduced with permission from ref 1. Copyright 2020 American Chemical Society.

the complex water adsorption on "realistic" oxide surfaces: after a first chemisorbed hydroxylated layer (can be typically stable up to 900 K), strongly bound, physisorbed icelike ordered water molecules (stable up to $T \sim 500$ K) are obtained. A higher coverage leads to chained polymer-like networks (decomposition at $T \leq 500$ K) before transitioning to a more weakly bound state similar to liquid H_2O (stable around $T < 300$ K).[1,17]

Carbon Reactivity

Essentially important for the fundamental understanding of carbon-fuel−catalyst interaction at high temperatures, the carbon reactivity is exemplified by the interaction of methane with clean Y_2O_3 and CO_2 with m-/t-ZrO_2.[2,3,11,18] Figure 4A shows, *via* correlated *in situ* FT-IR and EIS measurements, the distinct change of the surface at 1023 K by forming carbon deposits on the pure oxide surface (a common feature for all studied oxides), as indicated by both a drastic increase in conductivity by forming percolated carbon islands and an associated total decrease in IR transmission. Structurally, the carbon deposits are graphitic in nature, encapsulating grains and forming rosette-like morphologies (Figure 4B). Frequency-dependent EIS measurements (Figure 4C) reveal these carbon islands to be extremely dynamic, potentially also migrating to the metal−oxide interface in complexer systems, thus contributing to the overall reactivity of a combined metal−oxide catalyst entity. Similar interactions are observed for other C_1 molecules. Exemplified for t-ZrO_2, as shown in Figure 4D and E, a surface-carburizing high temperature treatment at 1273 K in CO_2 allows preservation of a complete surface-near ZrO_xC_y layer in an electron-conductive (oxy)carbidic-like state. Although the sample consists of >90 wt % m-ZrO_2 after the treatment, such a surface carburization is not obtained starting from m-ZrO_2 directly. Starting from t-ZrO_2, which is highly surface and bulk structurally defective (*e.g.*, exhibiting coordinatively unsaturated sites essentially arising from the synthesis procedure), hydroxylated, and more reactive, apparently strongly promotes these surface modifications. These studies further highlight the technological importance of understanding the interaction of simple SOFC entities with fuel components.[19] Even though coking is usually associated with the Ni content in traditional SOFC anodes,[10,11] our studies have revealed that at technologically relevant temperatures above ∼1000 K the oxidic component (*i.e.*, YSZ, but also ZrO_2 and Y_2O_3) is not exempt from this phenomenon either.[2,3]

In summary, these fundamental data on the adsorption and decomposition behavior of the basic constituents of reforming reactions on simple oxides already provide a foundation for subsequent stages in the experimental procedure, to explain reactivities obtained from catalytic testing in reforming reactions and to be used to project hypotheses onto compounds further along the complexity axis in the materials domain.

LEVEL 2: WATER AND CARBON REACTIVITY ON Y-DOPED ZrO_2: INFLUENCE OF THE Y-CONTENT ON REACTIVITY, SURFACE CONDUCTION AND CHEMISTRY IN C_1 GASES

On YSZ, chemically viewed simply as a solid solution of Y_2O_3 in ZrO_2, the surface-near water adsorption as a function of partial pressure is considerably more complex compared to that on simple ZrO_2 (Figure 5A), and also the multilayer water sorption is strongly different (Figure 5B). Above 80% relative humidity, an almost 10-fold increase in the amount of bound water is observed, whereas below that threshold the process is completely reversible without hysteresis, and only about 1% mass increase is observed (in contrast to pure ZrO_2, where only a mass change of 0.25% has been observed at close to 100% relative humidity). In due course, ZrO_2 appears rather hydrophobic, as it is much less hydroxylated than 8-YSZ (ZrO_2 stabilized with 8 mol % Y_2O_3[12]), which not only lowers the amount of water in the icelike layers, but essentially changes its binding mode. The higher amount of water in the icelike layer on YSZ can be attributed to the higher amount of OH groups and defects on the surface compared to ZrO_2. The scattered OH groups on the latter are, referenced to YSZ, too isolated to stabilize a total hydrogen-bound wetting of the surface. In contrast, on YSZ, pronounced stabilization of the

https://dx.doi.org/10.1021/acs.accounts.0c00218
Acc. Chem. Res. 2020, 53, 1811−1821

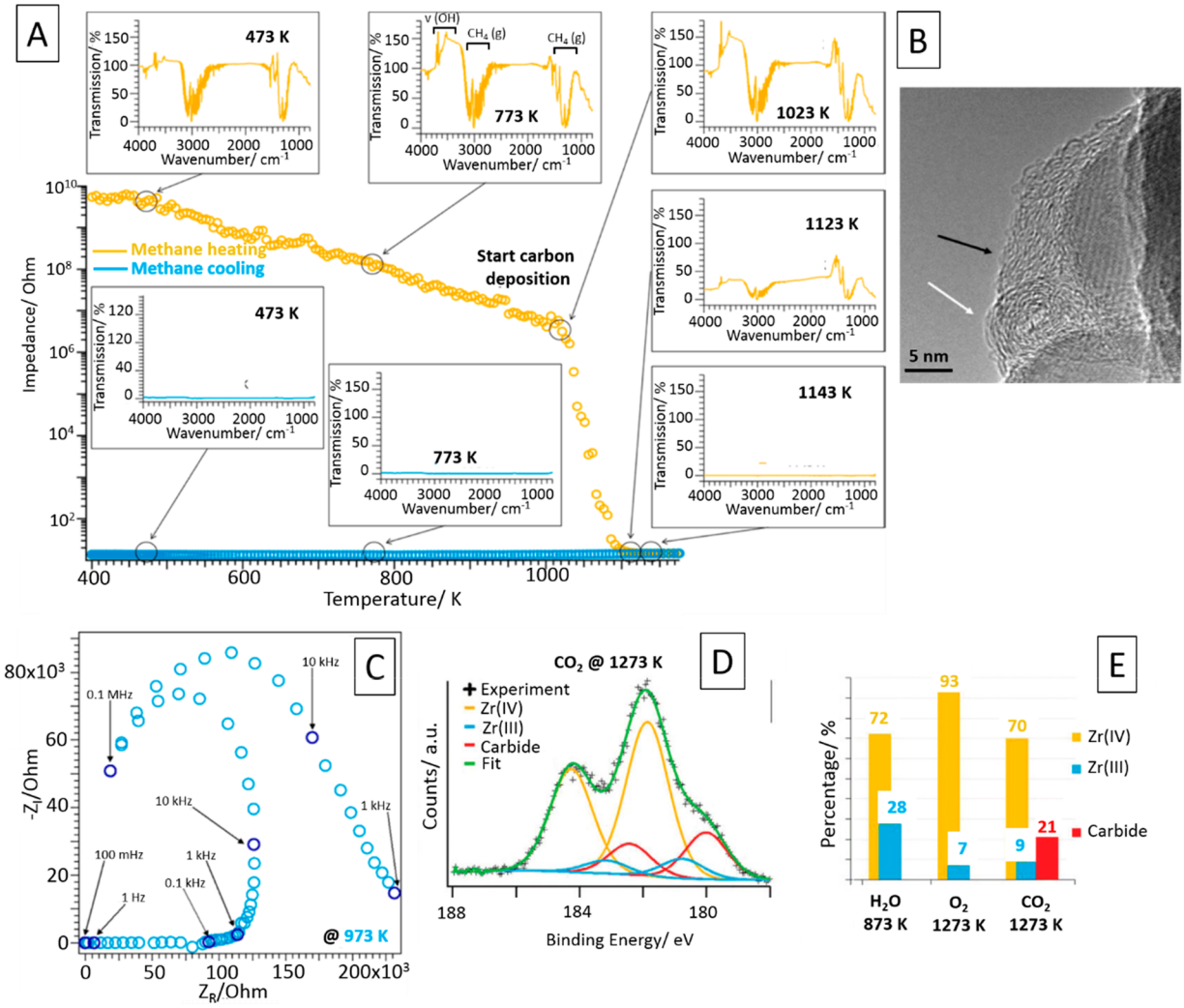

Figure 4. Carbon reactivity on $ZrO_2$and Y_2O_3: (A) Correlated *in situ* FT-IR and EIS data on Y_2O_3 during heating in methane up to 1143 K. (B) TEM image of a carbon-covered Y_2O_3 grain after exposure to methane at 1073 K. (C) Nyquist plot obtained during isothermal treatment of Y_2O_3 in methane at 973 K. (D) Deconvoluted Zr 3d XP spectrum after treatment of t-ZrO_2 in CO_2 at 1273 K. (E) Quantification of the surface species on t-ZrO_2 after various treatments. Reproduced from ref 18 (A,C), ref 3 (B), and ref 19 (D, E). Copyright 2016 the Royal Chemical Society, 2016 American Chemical Society, and 2017 the Royal Chemical Society, respectively.

OH-covered surface in the icelike layers is likely, increasing the capacity of water uptake in this specific layer relative to ZrO_2. It should be noted that different specific BET surface areas of these oxides lead to different mass changes and thus the absolute values cannot be compared. Nevertheless, the qualitative differences in the sorption experiments are representative, also corroborated by normalization of the water sorption to the respective surface area. Correlated *in situ* FT-IR and EIS data in 24 mbar water on 8-YSZ, referenced to measurements in dry He[1] and single- and polycrystalline YSZ to separate annealing and water adsorption effects,[20] indicate removal of water multilayers directly contributing to increased protonic conductivity, in vast difference to its pure oxidic counterparts, where the proton hopping mechanism proposed on YSZ is clearly absent.[21]

As for ZrO_2 and Y_2O_3, above ~1000 K, a strong interaction of C_1 gases with the YSZ surface was verified. Treatment in methane at 1173 K causes the formation of mostly graphitic deposits as revealed by transmission electron microscopy (TEM; Figure 5D). Raman spectroscopy on different spots on the surface allows the identification of a limited amount of nanotube-like features, indicating a considerable lateral heterogeneity of the carbon deposits across the surface (Figure 5E).[2,3] Combined admission of water and methane to simulate internal reforming gas atmospheres reveals a considerable larger amount of nanotube-like features, mostly due to the easier detachment of the carbon deposits from the YSZ grains (Figure 5F). In consequence, this leads to considerably different reactivity and surface chemical properties, as confirmed by corresponding FT-IR and EIS experiments.

Extension of these ideas and experiments to other doping levels to assess the entire ZrO_2–Y_2O_3 phase diagram reveals both similar features and vast differences. Carbon deposition during treatment in CH_4 at high temperatures $T \geq 1023$ K is a common feature, irrespective of the Y content (Figure 5G).[22] However, for all Y-doped samples temperature regions with different charge carrier activation energies could be identified, perfectly corresponding to significant changes in surface chemistry. Due to the different degree of hydroxylation and the different ability to chemisorb methane (but also CO and CO_2), the influence of the surface chemistry on the electro-

https://dx.doi.org/10.1021/acs.accounts.0c00218
Acc. Chem. Res. 2020, 53, 1811−1821

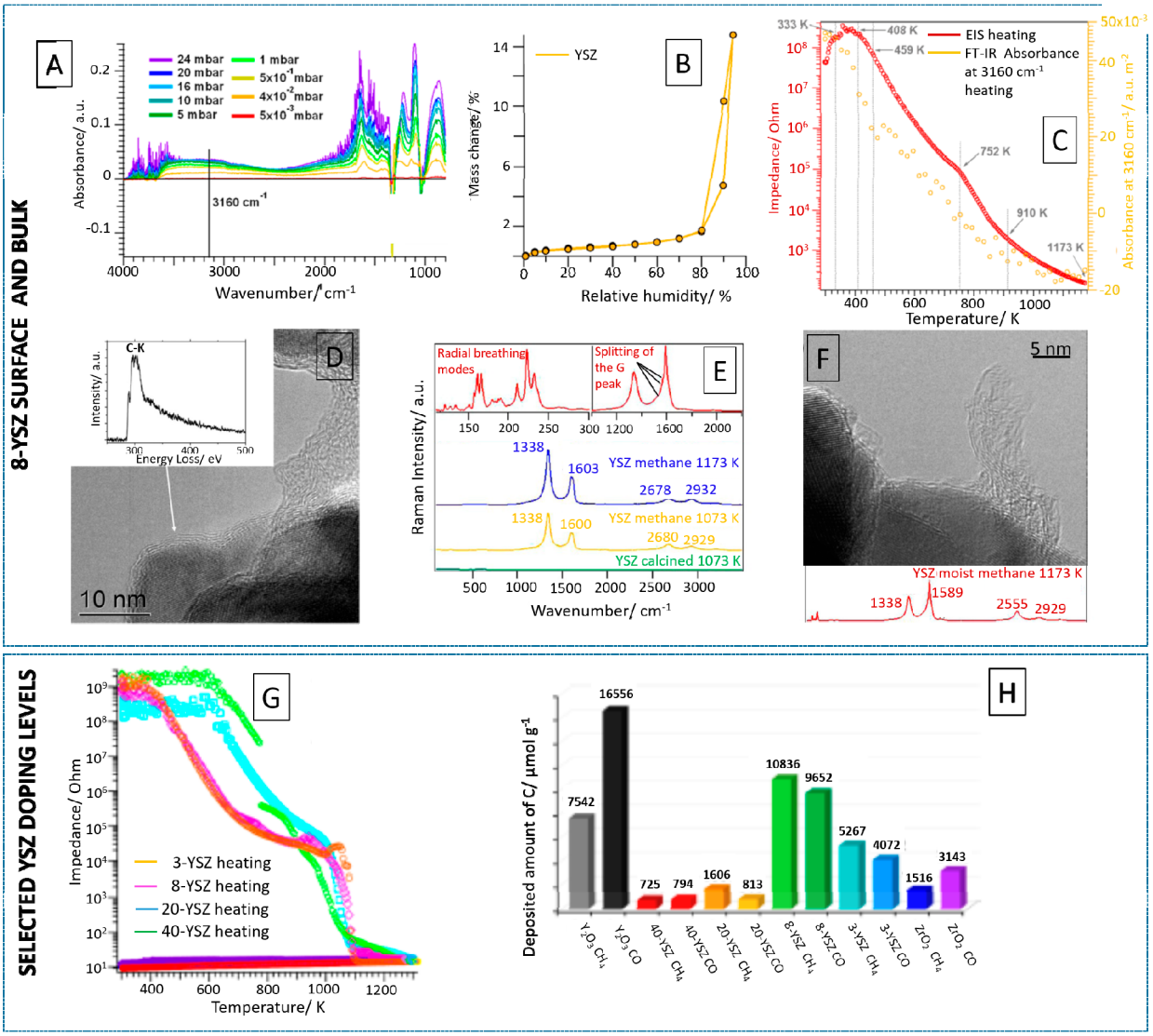

Figure 5. Water and carbon reactivity on Y-doped ZrO_2: (A) *In situ* isothermal FT-IR spectra during water exposure on 8-YSZ. (B) Dynamic water sorption on 8-YSZ. (C) Correlated *in situ* FT-IR–EIS data during heating 8-YSZ in pure methane to 1073 K. (D–F) TEM images and Raman spectra of the 8-YSZ surface after exposure to methane at 1073 K. (G) *In situ* EIS data collected during heating in methane up to 1073 K as a function of Y-doping. (H) Quantification of the carbon amount of doped YSZ samples after exposure to methane at 1073 K referenced to CO and pure Y_2O_3 and ZrO_2 (in μmol g^{-1}). Reproduced and adapted with permission from ref 1 (A–C), ref 3 (D–F), and ref 22 (G–H). Copyright 2016 American Chemical Society.

chemical properties and the amount of deposited carbon is varying strongly as a function of Y-content (Figure 5H).

LEVEL 3: THE IMPORTANCE OF WATER AND CARBON REACTIVITY ON Pd/ZrO_2 AND Cu/ZrO_2 METAL–OXIDE SYSTEMS DERIVED FROM *IN SITU* DECOMPOSED Pd–Zr AND Cu–Zr INTERMETALLIC COMPOUNDS AND ALLOY MATERIALS

The most complex systems described in this Account comprise Pd/ZrO_2 and Cu/ZrO_2 metal–oxide materials, obtained via controlled *in situ* decomposition of Pd_2Zr/Pd_3Zr bulk intermetallic compounds and a surface-near Pd–Zr alloy,[23] as well as $Cu_{51}Zr_{14}$ bulk materials in methane dry (DRM) and methanol steam reforming (MSR).[4,24]

Figure 6A displays XP spectra obtained on $Cu_{51}Zr_{14}$ after various catalytic runs in methanol steam reforming. The high CO_2 selectivity (referenced to both clean Cu and pure ZrO_2[24]), evident from the temperature-programmed catalytic profiles in Figure 6B, clearly goes along with differently reactive Zr-bound OH groups, whose binding energy matches those of t-ZrO_2 discussed previously. The overall Zr intensity diminishes as the Cu intensity increases. The structural reason for this is the complete decomposition of $Cu_{51}Zr_{14}$ in the water/methanol mixture, creating highly dispersed Cu particles at the surface in a matrix mostly consisting of t-ZrO_2 (Figure 6C). The initial intermetallic compound is therefore self-activating, and its corrosion product is highly CO_2 selective, which by *in situ* X-ray photoelectron spectroscopy (XPS) measurements has been attributed to the reversible formation of reactive surface-bound hydroxylated $Zr(OH)_x$ species. Thus, the *in situ* "selective" corrosion of the precatalyst's intermetallic compound state to at least partly form a metal/oxide system is a generally viable preparation pathway to active and selective catalyst materials, whose properties could only be fully understood once the

https://dx.doi.org/10.1021/acs.accounts.0c00218
Acc. Chem. Res. 2020, 53, 1811–1821

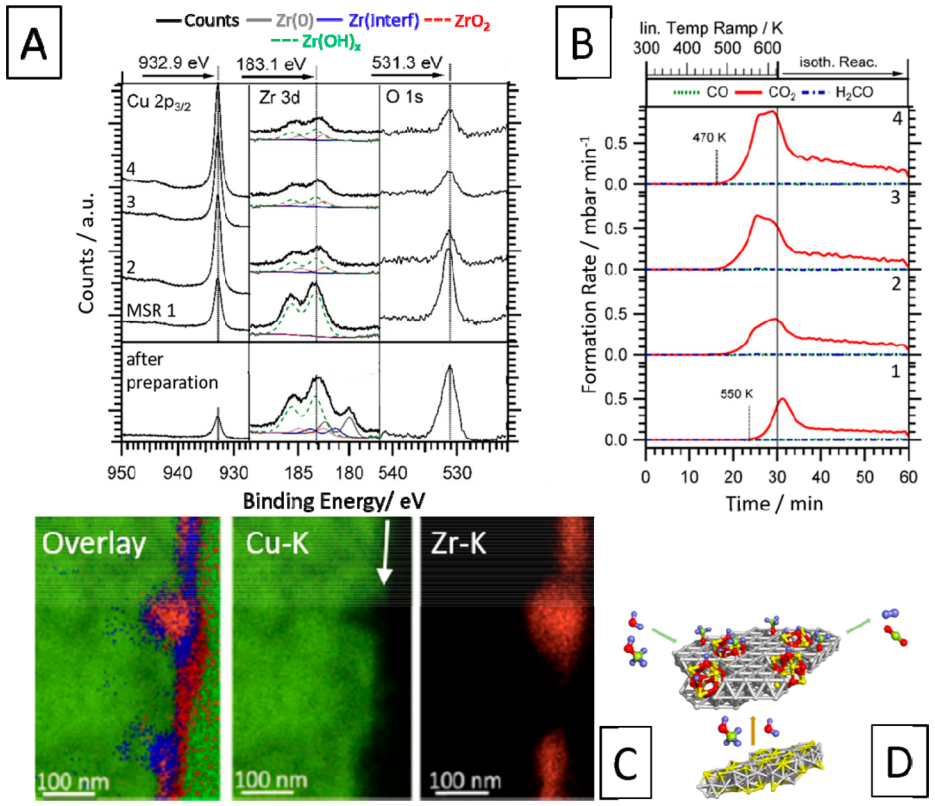

Figure 6. Water reactivity in MSR on Cu-ZrO_2: (A) XP spectra collected on the decomposed $Cu_{51}Zr_{14}$ intermetallic compound after several catalytic cycles 1−4. (B) Temperature-programmed catalytic profiles during four runs and complete decomposition of $Cu_{51}Zr_{14}$ (12 mbar methanol, 24 mbar water, 8 mbar Ar, backfilled with He to 1 bar total pressure; heating rate 10 K min^{-1}, geometric area of the sample: 3.6 cm^2). (C) Cross-sectional STEM-EDX data for $Cu_{51}Zr_{14}$ after the first catalytic run. The Cu−K and Zr−K images, as well as the overlay (including the O−K signal in blue), are highlighted. The arrow in the Cu−K map indicates the surface. (D) Schematic of the formation of Cu/t-ZrO_2 via decomposition of $Cu_{51}Zr_{14}$. (A−D) Reproduced with permission from refs 4 and 24. Copyright 2016 American Chemical Society and 2016 Wiley-VCH.

specific water reactivity of the oxidic component, as a prerequisite to CO_2 selective methanol steam reforming, has been assessed on previous levels of the work flow.

For Pd−ZrO_2, the composite metal−oxide state was obtained either by *in situ* decomposition of a Pd_2Zr/Pd_3Zr bulk intermetallic compound mixture or by forming a subsurface Pd−Zr alloy by reductive dissolution of chemical vapor-deposited ZrO_x species into a Pd foil.[23,25] The reactivities of both systems in the dry reforming of methane (DRM) reaction are vastly different: the CO formation rate is significantly higher on the bulk-derived Pd/ZrO_x system (peaking at about 8.5 hPa min^{-1}, Figure 7A) than on the on the subsurface alloy (0.3 hPa min^{-1}, *cf.* referenced to the reactivity on clean Pd and ZrO_2 also shown in both graphs, Figure 7A and C). The latter barely exceeds the activity of pure ZrO_2. *Operando* near-ambient-pressure XPS (Figure 7B and D) indicates a characteristic carbon morphology on Pd/ZrO_2 followed by *in situ* decomposition of Pd_2Zr/Pd_3Zr. Exclusively for the latter, a carbidic Pd component (green labeled in the deconvoluted Pd 3d and C 1s spectra) is visible in different CH_4/CO_2 mixtures. This is attributed to the different Pd grain sizes: for the subsurface alloy, the active phase exhibits a large interface to a bulk Pd foil acting as a quasi-infinite reservoir to store carbon. Any carbon formed due to decomposition of methane is immediately dissolved into the bulk, whereas the small Pd nanoparticles present in the decomposed bulk intermetallic compound have a limited storage capacity for carbon, leading to fast saturation.[23] Thus, the observed higher activity can be explained by a catalytic spillover effect, as displayed in the inset in Figure 7A. Methane is decomposed on the Pd surface, essentially leading to the dissolution of reactive carbon into Pd and its effective migration to the Pd/ZrO_2 interface, reacting there with adsorbed/activated CO_2 via the reverse Boudouard reaction. Without carbon supersaturation of Pd, the statistical probability of the latter process will be negligibly small. By this means, the reduced Pd dimensions invoke higher CO formation rates on Pd_2Zr/Pd_3Zr, characterized by smaller Pd nanoparticles in contact with ZrO_2 (formed *in situ*), relative to the subsurface alloy. An at least limited reducibility of ZrO_2 by carbon around 1000 K at the interface is required for the proposed assistance of Zr(ox) sites in CO_2 activation and the transfer of CO_2-derived oxygen to the latter (following fast supply of reactive C atoms toward the phase boundary), which was essentially derived on level 1 for pure ZrO_2.[23]

We have shown how the knowledge derived on levels 1 and 2 with respect to the material and catalytic properties can help to elucidate reaction mechanisms on materials of the highest complexity, featuring interfaces between metals, oxides, and, in the case of only partial decomposition, also alloys/intermetallic compounds. As the latter represent structurally highly dynamic systems, decomposing at least partly into a metal−oxide composite, knowledge about the constituting entities is imperative, directly validating our increasing complexity approach.

https://dx.doi.org/10.1021/acs.accounts.0c00218
Acc. Chem. Res. 2020, 53, 1811−1821

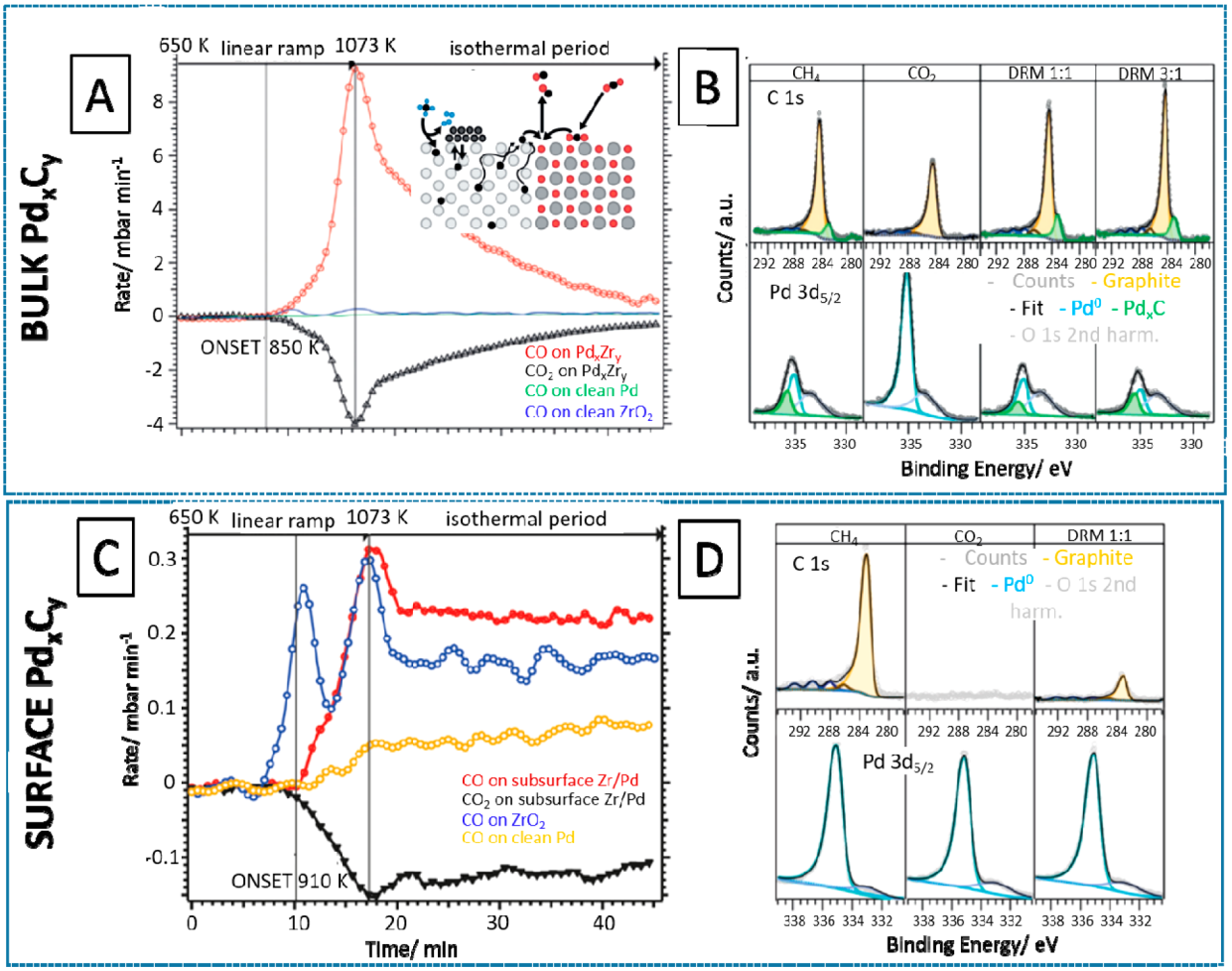

Figure 7. Carbon reactivity in DRM on Pd-ZrO_2: (A) CO formation rates and (B) *operando* NAP-XP spectra for an intermetallic Pd_2Zr/Pd_3Zr system during DRM. Proposed reaction scheme for the reactivity of the decomposed intermetallic Pd_2Zr/Pd_3Zr material shown as an inset. (C) CO formation rates and (D) *operando* NAP-XP spectra for a surface alloy Pd_xZr_y system during DRM. (A–D) Reproduced ith permission from ref 23. Copyright 2018 Wiley-VCH.

Although only two examples are presented on level 3, the possibilities in using selected intermetallic compounds to act as catalyst precursors to prepare highly active and CO_2-selective reforming catalyst entities by controlled *in situ* decomposition can be generalized. An obvious prerequisite is the at least partial mutual solubility to from alloys or even intermetallic compounds. Prominent examples fulfilling these requirements include CuZn,[26] $GaPd_2$,[27] Cu_2In,[28] or ZnPd.[29] The common feature of all systems is the combination of a noble metal, which eventually remains in its metallic state, with an unnoble/depassivated metal that is likely to be oxidized upon decomposition, thus forming the metal–oxide interface. The overall activation process, thus, corresponds to the classical picture of "selective corrosion" of an intermetallic compound or alloy surface and bulk structure and is accompanied by the *in situ* formation of much more complex catalyst entities. These rearrangements can be present in the form of a complete destruction of the intermetallic compound bulk structure ($Cu_{51}Zr_{14}$),[4,24] the formation of an metal/oxide ($Cu_{51}Zr_{14}$) or intermetallic compound/oxide (ZnPd, Cu_2In, CuZn) interface, or the intertransformation of intermetallic compounds with varying composition (Pd_2Zr) during decomposition. A common leading theme is also the intrinsic reactivity of the resulting oxide (or the metal–oxide interface) in the metal–oxide system.[30−35] Surface chemical aspects, including the discussed propensity to adsorb (and activate) water *e.g.* for steam reforming or form reactive carbon species in dry reforming govern the catalytic properties of the oxide and thus, influence the catalytic performance of the entire catalyst detrimentally or beneficially. Other obvious key criteria include the oxidation propensity and general thermodynamic stability of the chosen intermetallic compound/alloy or the metastability of the evolving oxide polymorph that is formed upon decomposition.

SUMMARY AND PERSPECTIVE

Exemplifying the use of SOFC anode materials and their surface and bulk chemistry relevant for different (internal) reforming processes, we have demonstrated a comprehensive workflow using a knowledge-based survey of the materials space, sampling different levels of complexity. Complexity in this case refers to chemical composition, applied experimental techniques, and catalytic reactions.

ZrO_2, Y_2O_3, and YSZ (representing complexity levels 1 for ZrO_2/Y_2O_3 and 2 for YSZ) were exemplarily investigated with respect to their behavior upon water adsorption and carbon chemistry/methane reactivity. By considering the fundamental building blocks of reforming catalysts, it was shown that the

https://dx.doi.org/10.1021/acs.accounts.0c00218
Acc. Chem. Res. 2020, 53, 1811−1821

water and carbon reactivity are very different among these materials, leading to different adsorbate species. These encompass chemisorbed H_2O, physisorbed icelike layers and almost liquidlike water, as well as different carbon morphologies as a function of atmosphere and doping level. In fact, also the isolated oxide materials are prone to coking and have the ability to form carbon filament- and nanotube-like features, causing in part deactivation at typical operating temperatures above 1073 K. This is especially important for the use of conventional SOFC Ni/YSZ cermet anodes, where coking is essentially attributed to the nickel species (exhibiting a higher coking propensity than oxides[8]).

Increasing the complexity also along the experimental axis, starting from fundamental studies on the single and isolated components, subsequently lifting the restriction of focusing on the effect of a single component, leads to a deeper knowledge about the catalytic properties of more complex materials. Moving to the highest complexity level 3, the common activity and selectivity descriptor in methane dry and methanol steam reforming over metal−oxide systems derived from *in situ* corrosion of intermetallic compounds and alloys is the specific water-, CO_2-, and carbon-activating function of the individual components, providing the connection to the reactivity studies described on level 1. With respect to water reactivity, the studies in methanol steam reforming not only directly help in interpreting the adsorbed OH features at lower temperatures, but our studies also showed that some water species even persist on the oxide surface at reforming- and/or SOFC-relevant temperatures, with strikingly different properties than those present at lower temperatures. With respect to the up to now unknown surface reducibility of ZrO_2 (either via carburization to an (oxy)carbide or in hydrogen (not shown in detail, but equally possible[36]) and the associated defect chemistry for water activation and CO_2 reforming, we provided another example for the knowledge transfer between the levels: only by assessment of the pure oxide-bound surface and interface surface reduction can a "carbothermal" defect chemistry at the phase boundary be postulated for the methane dry reforming reaction and the carbon source pinpointed at Pd−only the combination of both will eventually yield a complete picture of the reaction mechanism. Elucidating the reactivity of the phase boundary of a metal to a doped oxide by using the knowledge of level 2, would be the next logical step in the direct knowledge transfer between levels 2 and 3.

Entangled with the workflow regarding material complexity, we emphasize the necessity for the use of *in situ* and *operando* structure-determining and spectroscopic techniques, such as *in situ* X-ray diffraction, *in situ* X-ray absorption spectroscopy, or *in situ* FT-infrared and *in situ* electrochemical impedance spectroscopy. Only the combination of such methods allows one to derive a clear picture of the interplay of reactants and surfaces and its structural, morphological, or catalytic consequences. We have chosen one illustrative example of water and carbon reactivity relevant for SOFC anode chemistry on different levels of materials complexity, but by taking in the principles worked out for this particular example, generalization to more complex materials or reactions is possible.

AUTHOR INFORMATION

Corresponding Author

Simon Penner − *Department of Physical Chemistry, University Innsbruck, 6020 Innsbruck, Austria;* orcid.org/0000-0002-2561-5816; Email: simon.penner@uibk.ac.at

Authors

Thomas Götsch − *Department of Inorganic Chemistry, Fritz Haber Institute of the Max Planck Society, 14195 Berlin, Germany; Department of Heterogeneous Reactions, Max Planck Institute for Chemical Energy Conversion, 45470 Mülheim an der Ruhr, Germany; Department of Physical Chemistry, University Innsbruck, 6020 Innsbruck, Austria;* orcid.org/0000-0003-3673-317X

Bernhard Klötzer − *Department of Physical Chemistry, University Innsbruck, 6020 Innsbruck, Austria*

Complete contact information is available at: https://pubs.acs.org/10.1021/acs.accounts.0c00218

Author Contributions

The manuscript was written through contributions of all authors. All authors have given approval to the final version of the manuscript.

Funding

This work was partly funded by the Austrian Science Fund (FWF) via Grant F4503-N16. T.G. acknowledges additional funding by the Deutsche Forschungsgemeinschaft (DFG, German Research Foundation) − Projektnummer 388390466 − TRR 247 as well as by the Austrian Science Fund (FWF) via Grant J4278-N37.

Notes

The authors declare no competing financial interest.

Biographies

Simon Penner. Born in 1975 in Innsbruck (Austria), he obtained his PhD from the University of Innsbruck in 2004 on the topic of electron microscopy analysis of the metal−support interaction in noble metal−oxide systems. He obtained his habilitation in Physical Chemistry in 2011 and is currently working as a senior scientist at the Institute of Physical Chemistry at the University of Innsbruck. His research interests lie predominantly in the *in situ* and *operando* structural and spectroscopic characterization of complex oxide, metal−oxide and intermetallic compounds as heterogeneous catalysts.

Thomas Götsch. Born in 1991 in Zams (Austria), he obtained his PhD from the University of Innsbruck in 2018, where he investigated complex oxides used in solid oxide fuel cells. Currently, he is working as a Post-Doc at the Department of Inorganic Chemistry at the Fritz Haber Institute of the Max Planck Society in Berlin, Germany. There, he is focusing on *in situ* and *operando* photoelectron spectroscopy and electron microscopy studies of the oxygen evolution reaction in alkaline and solid oxide electrolytes, as well as low temperature alcohol oxidation reactions and solid oxide fuel cells.

Bernhard Klötzer is associated professor at the Institute of Physical Chemistry at the University of Innsbruck. Obtaining his habilitation in Physical chemistry in 2011, he has a long-standing expertise in synchrotron-based *in situ*/*operando* near ambient pressure (NAP)-XPS characterization of catalytically active states, application of NAP-XPS to model solid oxide (SOC) cells, experimental development of high temperature *in situ*/*operando* DRIFTS, and FT-IRAS characterization

https://dx.doi.org/10.1021/acs.accounts.0c00218
Acc. Chem. Res. 2020, 53, 1811−1821

of SOC electrodes/materials at high temperatures, combined with online electrical impedance (EIS) electrode characterization.

■ ABBREVIATIONS

DRM, dry reforming of methane; EDX, energy-dispersive X-ray spectroscopy; EIS, electrochemical impedance spectroscopy; FTIR, Fourier transform infrared spectroscopy; MSR, methanol steam reforming; SOEC, solid oxide electrolysis cell; SOFC, solid oxide fuel cell; SRM, steam reforming of methane; (S)TEM, (scanning) transmission electron microscopy; XRD, X-ray diffraction; YSZ, yttria-stabilized zirconia

■ REFERENCES

(1) Köck, E.-M.; Kogler, M.; Klötzer, B.; Noisternig, M. F.; Penner, S. Structural and Electrochemical Properties of Physisorbed and Chemisorbed Water Layers on the Ceramic Oxides Y_2O_3, YSZ, and ZrO_2. *ACS Appl. Mater. Interfaces* **2016**, *8*, 16428−16443.

(2) Kogler, M.; Köck, E.-M.; Perfler, L.; Bielz, T.; Stöger-Pollach, M.; Hetaba, W.; Willinger, M.; Huang, X.; Schuster, M.; Klötzer, B.; Penner, S. Methane Decomposition and Carbon Growth on Y_2O_3, Yttria-Stabilized Zirconia, and ZrO_2. *Chem. Mater.* **2014**, *26*, 1690−1701.

(3) Kogler, M.; Köck, E.-M.; Klötzer, B.; Perfler, L.; Penner, S. Surface Reactivity of YSZ, Y_2O_3 and ZrO_2 toward CO, CO_2 and CH_4: A Comparative Discussion. *J. Phys. Chem. C* **2016**, *120*, 3882−3898.

(4) Mayr, L.; Köpfle, N.; Klötzer, B.; Götsch, T.; Bernardi, J.; Schwarz, S.; Keilhauer, T.; Armbrüster, M.; Penner, S. Microstructural and Chemical Evolution and Analysis of a Self-Activating CO_2-Selective Cu−Zr Bimetallic Methanol Steam Reforming Catalyst. *J. Phys. Chem. C* **2016**, *120*, 25395−25404.

(5) Nehter, P.; Wildrath, B.; Bauschulte, A.; Leites, K. Diesel Based SOFC Demonstrator for Maritime Applications. *ECS Trans.* **2017**, *78*, 171−180.

(6) Shiratori, Y.; Ijichi, T.; Oshima, T.; Sasaki, K. Internal Reforming SOFC Running on Biogas. *Int. J. Hydrogen Energy* **2010**, *35*, 7905−7912.

(7) Clarke, S. H.; Dicks, A. L.; Pointon, K.; Smith, T. A.; Swann, A. Catalytic Aspects of the Steam Reforming of Hydrocarbons in Internal Reforming Fuel Cells. *Catal. Today* **1997**, *38*, 411−423.

(8) Toebes, M. Impact of the Structure and Reactivity of Nickel Particles on the Catalytic Growth of Carbon Nanofibers. *Catal. Today* **2002**, *76*, 33−42.

(9) Götsch, T.; Schachinger, T.; Stöger-Pollach, M.; Kaindl, R.; Penner, S. Carbon Tolerance of Ni−Cu and Ni−Cu/YSZ Sub-μm Sized SOFC Thin Film Model Systems. *Appl. Surf. Sci.* **2017**, *402*, 1−11.

(10) McIntosh, S.; Gorte, R. J. Direct Hydrocarbon Solid Oxide Fuel Cells. *Chem. Rev.* **2004**, *104*, 4845−4866.

(11) Kim, T.; Liu, G.; Boaro, M.; Lee, S.-I.; Vohs, J. M.; Gorte, R. J.; Al-Madhi, O. H.; Dabbousi, B. O. A Study of Carbon Formation and Prevention in Hydrocarbon-Fueled SOFC. *J. Power Sources* **2006**, *155*, 231−238.

(12) Götsch, T.; Wallisch, W.; Stöger-Pollach, M.; Klötzer, B.; Penner, S. From Zirconia to Yttria: Sampling the YSZ Phase Diagram Using Sputter-Deposited Thin Films. *AIP Adv.* **2016**, *6*, 025119.

(13) Drazin, J. W.; Castro, R. H. R. Phase Stability in Nanocrystals: A Predictive Diagram for Yttria-Zirconia. *J. Am. Ceram. Soc.* **2015**, *98*, 1377−1384.

(14) Holgado, J.P.; Escobar Galindo, R.; van Veen, A.; Schut, H.; de Hosson, J.Th.M.; Gonzalez-Elipe, A.R. Structural Effects Due to the Incorporation of Ar Atoms in the Lattice of ZrO_2 Thin Films Prepared by Ion Beam Assisted Deposition. *Nucl. Instrum. Methods Phys. Res., Sect. B* **2002**, *194*, 333−345.

(15) Kogler, M.; Köck, E.-M.; Vanicek, S.; Schmidmair, D.; Götsch, T.; Stöger-Pollach, M.; Hejny, C.; Klötzer, B.; Penner, S. Enhanced Kinetic Stability of Pure and Y-Doped Tetragonal ZrO_2. *Inorg. Chem.* **2014**, *53*, 13247−13257.

(16) Lackner, P.; Hulva, J.; Köck, E.-M.; Mayr-Schmölzer, W.; Choi, J.; Penner, S.; Diebold, U.; Mittendorfer, F.; Redinger, S.; Klötzer, B.; Parkinson, G.; Schmid, M. Water Adsorption at Zirconia: from the $ZrO_2(111)Pt_3Zr(0001)$ Model System to Powder Samples. *J. Mater. Chem. A* **2018**, *6*, 17587−17601.

(17) Henderson, M. The Interaction of Water with Solid Surfaces: Fundamental Aspects Revisited. *Surf. Sci. Rep.* **2002**, *46*, 1−308.

(18) Köck, E.-M.; Kogler, M.; Götsch, T.; Klötzer, B.; Penner, S. Structural and Chemical Degradation Mechanisms of pure YSZ and its Components ZrO_2 and Y_2O_3 in Carbon-Rich fuel Gases. *Phys. Chem. Chem. Phys.* **2016**, *18*, 14333−14349.

(19) Köck, E.-M.; Kogler, M.; Götsch, T.; Schlicker, L.; Bekheet, M. F.; Doran, A.; Gurlo, A.; Klötzer, B.; Petermüller, B.; Schildhammer, D.; Yigit, N.; Penner, S. Surface Chemistry of Pure Tetragonal ZrO_2 and Gas Phase-Dependence of the Tetragonal-to-Monoclinic ZrO_2 Transformation. *Dalton Trans.* **2017**, *46*, 4554−4570.

(20) Ahamer, C.; Opitz, A. K.; Rupp, G. M.; Fleig, J. Revisiting the Temperature Dependent Ionic Conductivity of Yttria Stabilized Zirconia (YSZ). *J. Electrochem. Soc.* **2017**, *164*, F790−F803.

(21) Raz, S.; Sasaki, K.; Maier, J.; Riess, I. Characterization of Adsorbed Water Layers on Y_2O_3-doped ZrO_2. *Solid State Ionics* **2001**, *143*, 181−204.

(22) Kogler, M.; Köck, E.-M.; Klötzer, B.; Penner, S. Structure-Property Relationships in the Y_2O_3-ZrO_2 Phase Diagram: Influence Of the Y-Content on Reactivity in C1 Gases, Surface Conductivity and Surface Chemistry. *J. Phys. Chem. C* **2016**, *120*, 22443−22454.

(23) Köpfle, N.; Götsch, T.; Grünbacher, M.; Carbonio, E. A.; Hävecker, M.; Knop-Gericke, A.; Schlicker, L.; Doran, A.; Kober, D.; Gurlo, A.; Penner, S.; Klötzer, B. Zirconium-Assisted Activation of Palladium To Boost Syngas Production by Methane Dry Reforming. *Angew. Chem., Int. Ed.* **2018**, *57*, 14613−14618.

(24) Mayr, L.; Klötzer, B.; Schmidmair, D.; Köpfle, N.; Bernardi, J.; Schwarz, S.; Armbrüster, M.; Penner, S. Boosting Hydrogen Production from Methanol and Water by In Situ Activation of Bimetallic Cu-Zr Species. *ChemCatChem* **2016**, *8*, 1778−1781.

(25) Köpfle, N.; Mayr, L.; Schmidmair, D.; Bernardi, J.; Knop-Gericke, A.; Hävecker, M.; Klötzer, B.; Penner, S. A Comparative Discussion of the Catalytic Activity and CO2□Selectivity of Cu□Zr and Pd□Zr (Intermetallic) Compounds in Methanol Steam Reforming. *Catalysts* **2017**, *7*, 53−70.

(26) Rameshan, C.; Stadlmayr, W.; Penner, S.; Lorenz, H.; Memmel, N.; Hävecker, M.; Blume, R.; Teschner, D.; Rocha, T.; Zemlyanov, D.; Knop-Gericke, A.; Schlögl, R.; Klötzer, B. Hydrogen Production by Methanol Steam Reforming on Copper Boosted by Zinc-Assisted Water Activation. *Angew. Chem., Int. Ed.* **2012**, *51*, 3002−3006.

(27) Mayr, L.; Lorenz, H.; Armbrüster, M.; Villaseca, S.; Luo, Y.; Cardoso, R.; Burkhardt, U.; Zemlyanov, D.; Haevecker, M.; Blume, R.; Knop-Gericke, A.; Klötzer, B.; Penner, S. The Catalytic Properties of Thin Film Pd-Rich $GaPd_2$ in Methanol Steam Reforming. *J. Catal.* **2014**, *309*, 231−240.

(28) Ploner, K.; Schlicker, L.; Gili, A.; Gurlo, A.; Doran, A.; Zhang, L.; Armbrüster, M.; Obendorf, D.; Bernardi, J.; Klötzer, B.; Penner, S. Reactive Metal-Support Interaction in the Cu-In_2O_3 System: Intermetallic Compound Formation and its Consequences for CO_2-Selective Methanol Steam Reforming. *Sci. Technol. Adv. Mater.* **2019**, *20*, 356−366.

(29) Friedrich, M.; Penner, S.; Heggen, M.; Armbrüster, M. High CO_2 Selectivity in Methanol Steam Reforming through ZnPd/ZnO Teamwork. *Angew. Chem., Int. Ed.* **2013**, *52*, 4389−4392.

(30) Lorenz, H.; Jochum, W.; Klötzer, B.; Stöger-Pollach, M.; Schwarz, S.; Pfaller, K.; Penner, S. Novel Methanol Steam Reforming Activity and Selectivity of Pure In_2O_3. *Appl. Catal., A* **2008**, *347*, 34−42.

(31) Jochum, W.; Penner, S.; Kramer, R.; Föttinger, K.; Rupprechter, G.; Klötzer, B. Defect Formation and the Water−Gas Shift Reaction on β-Ga_2O_3. *J. Catal.* **2008**, *256*, 278−286.

(32) Jochum, W.; Penner, S.; Föttinger, K.; Kramer, R.; Rupprechter, G.; Klötzer, B. Hydrogen on Polycrystalline β-Ga_2O_3: Surface

https://dx.doi.org/10.1021/acs.accounts.0c00218
Acc. Chem. Res. 2020, 53, 1811−1821

Chemisorption, Defect Formation, and Reactivity. *J. Catal.* **2008**, *256*, 268−277.
(33) Bielz, T.; Lorenz, H.; Jochum, W.; Kaindl, R.; Klauser, F.; Klötzer, B.; Penner, S. Hydrogen on In_2O_3: Reducibility, Bonding, Defect Formation, and Reactivity. *J. Phys. Chem. C* **2010**, *114*, 9022−9029.
(34) Bielz, T.; Lorenz, H.; Amann, P.; Klötzer, B.; Penner, S. Water-Gas Shift and Formaldehyde Reforming Activity Determined by Defect Chemistry of Polycrystalline In_2O_3. *J. Phys. Chem. C* **2011**, *115*, 6622−6628.
(35) Lorenz, H.; Friedrich, M.; Armbrüster, M.; Klötzer, B.; Penner, S. ZnO is a CO_2-Selective Steam Reforming Catalyst. *J. Catal.* **2013**, *297*, 151−154.
(36) Kogler, M.; Köck, E.-M.; Bielz, T.; Pfaller, K.; Klötzer, B.; Schmidmair, D.; Perfler, L.; Penner, S. Hydrogen Surface Reactions and Adsorption Studied on Y_2O_3, YSZ, and ZrO_2. *J. Phys. Chem. C* **2014**, *118*, 8435−8444.

https://dx.doi.org/10.1021/acs.accounts.0c00218
Acc. Chem. Res. 2020, 53, 1811−1821